Journal of Alloys and Compounds 499 (2010) 194–199

Contents lists available at ScienceDirect

Journal of Alloys and Compounds

journal homepage: www.elsevier.com/locate/jallcom

The Zn-rich corner of the Zn–Al–Ti system at 723 K

Sui Yang[a,c], Xuping Su[c,b,*], Jianhua Wang[c], Fucheng Yin[c], Zhi Li[c], Hao Tu[c], Haoping Peng[c]

[a] Faculty of Materials, Optoelectronics and Physics, Xiangtan University, Xiangtan, 411105 Hunan, PR China
[b] School of Materials Science and Engineering, Jiangsu Polytechnic University, Changzhou, 213164 Jiangsu, PR China
[c] Key Laboratory of Materials Design and Preparation Technology of Hunan Province, Xiangtan University, Xiangtan, 411105 Hunan, PR China

ARTICLE INFO

Article history:
Received 13 November 2009
Received in revised form 17 March 2010
Accepted 17 March 2010
Available online 23 March 2010

Keywords:
Zn–Al–Ti system
Phase diagram
Zn-rich corner
Galvanizing

ABSTRACT

The Zn-rich corner of the Zn–Al–Ti ternary system at 723 K was experimentally determined using equilibrated alloys with the aid of diffusion couple approach. The specimens were investigated by means of optical microscopy, scanning electron microscopy, wave dispersive X-ray spectroscope and X-ray powder diffraction. A true ternary phase T was identified and it is in equilibrium with $TiAl_3$, $TiAl_2$, α-Al, liq.Zn, $TiZn_{16}$, $TiZn_8$ and TiZn in the system respectively. The solubility of Ti in liquid zinc is 0.3 at.%. The solubility of Zn in $TiAl_3$ and $TiAl_2$ is 4.4 at.% and 3.2 at.% respectively and that of Al in $TiZn_{16}$, $TiZn_8$, $TiZn_3$ and TiZn is 0.4 at.%, 0.2 at.%, 1.7 at.% and 2.5 at.% respectively.

1. Introduction

Zinc and zinc alloy are often used as donor materials for depositing protective coating on a variety of ferrous substrates to improve the corrosion resistance [1]. Hot-dip galvanizing technique is applied by dipping the steels in the molten zinc or its alloys either in a continuous manner or by a batch process [2]. Silicon is one of the most important elements added to steel, and its influence is traduced by the well known "Sandelin" phenomenon which is generally associated with the production of thick coatings, unsightly surface defects, often rejected as a result of their poor mechanical properties [3]. A practical solution to this problem is galvanizing the steels in alloyed baths. The primary alloying element used in the galvanizing industry is aluminum [4]. The addition of aluminum resulting in the formation of an inhibition layer of Fe–Al intermetallic compound on the surface of the steel eliminates the Sandelin phenomenon. Most recent investigation on continuous galvanizing of Ti-stabilized interstitial-free steels showed that an interface layer of $Fe_2Al_{5-x}Zn_x$ formed immediately upon the contact of the incoming strip with the molten Zn–Al alloy [5]. Some other element such as titanium was introduced into zinc bath to control the excessive reactivity induced by the Si contained in the steel [6,7]. The Sandelin phenomenon disappears when small amount of titanium is added to the zinc bath at 723 K [6]. However, large amount of titanium in the liquid phase could lead to defected coatings and excessive dross precipitation [7]. The synergistic effect of Al and Ti on the structure and the surface quality of the coating has been investigated [8]. The results showed that the addition of titanium could serve as a catalyst for the Fe–Al reaction, allowing a greater development of the inhibition layer and delaying growth of the Fe–Zn intermetallic.

The control of equilibrium between the liquid phase (zinc bath) and the solid phase (intermetallics both the galvanized coating and precipitates in the bath) requires the knowledge of the Fe–Zn–Al–Ti phase diagram, especially in the Zn-rich corner, at the temperature relevant to hot-dip galvanizing. However, the development of this quaternary diagram first requires the study of the three other ternary diagrams in the zinc-rich corner. The Fe–Zn–Al diagram has been thoroughly assessed by different authors [9,10]. The Fe–Zn–Ti system has been experimentally investigated recently [11]. However, the information of phase equilibria in the Zn–Al–Ti ternary system was not reported. Hence, the purpose of the present study is to experimentally determine the Zn–Al–Ti isothermal section at 723 K with an emphasis on the Zn-rich corner.

Among the binaries constituting the ternary Zn–Al–Ti system, the Zn–Al and Ti–Al phase diagrams are well determined while the Zn–Ti phase diagram is not well studied. The Zn–Al system is an eutectic system involving a monotectoid reaction and a miscibility gap in the solid state [12]. No intermediate compound and only three condensed phases: liquid, Al-based FCC and Zn-based hcp solid solution are available in the system. The thermodynamic and phase equilibrium data were critically assessed by Murray [13].

* Corresponding author at: Key Laboratory of Materials Design and Preparation Technology of Hunan Province, Xiangtan University, Xiangtan, 411105 Hunan, PR China. Tel.: +86 731 58292213; fax: +86 731 58292210.
E-mail address: sxping@xtu.edu.cn (X. Su).

0925-8388/$ – see front matter © 2010 Elsevier B.V. All rights reserved.
doi:10.1016/j.jallcom.2010.03.148

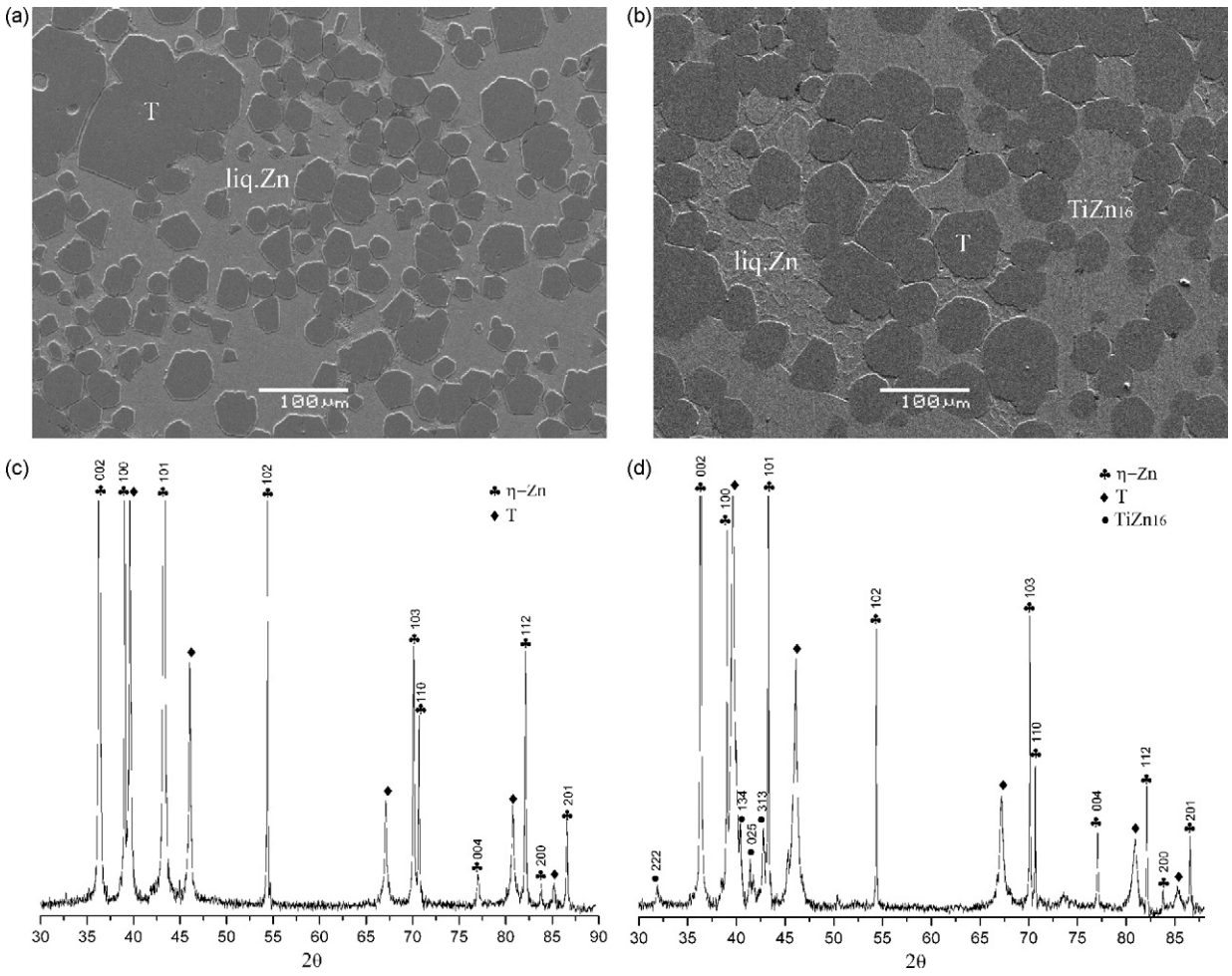

Fig. 1. SEM images and XRD patterns of the Alloys 1 and 2 annealed at 723 K for 30 days. (a) The microstructure of Alloy 1 consists of two phases, the T phase and liq.Zn phase. (b) SEM image of Alloy 2 corresponds to the three-phase equilibrium state of T + $TiZn_{16}$ + liq.Zn. (c) XRD pattern of Alloy 1. (d) XRD pattern of Alloy 2.

However, the calculated phase diagram was not in good agreement with the experimental data available in the literature and the types of models used for the different phases were not mentioned. Subsequently, the thermodynamics of the system was re-evaluated by Mey and Effenberg [14]. But the calculated phase boundary of the miscibility gap of the FCC phase differs markedly from the experimental data. A recent assessment of the experimental data and re-optimization of the binary Zn–Al system [15] has been performed which considers the presence of short-range order in the liquid phase as well as in the Al-FCC solid solution phase. This calculated phase diagram which shows a reasonable agreement with the experimental data from the literature is accepted in the present work.

Contributing to the low density, high strength and good plastic properties, the Ti–Al alloys have prospective applications in the aviation and automotive industries. Since early in 1923, Erkelenz [16] had investigated the phase relationship of the Ti–Al system. However, the early limitations in theoretical models restricted the application of the thermodynamic phase diagram calculations. It has been almost 30 years since a detailed presentation on thermodynamic phase diagram calculations for Ti–Al system was presented by Kaufman and Nesor [17] at the 2nd World Confer-

Table 1
Crystallographic data of the binary compounds in the Zn–Al–Ti ternary system.

Compound	Space group	Structure type	Lattice parameters (Å)			Reference
			a	*b*	*c*	
$TiAl_3$	*I*4/*mmm*	Al_3Ti	3.853		8.583	[36]
$TiAl_2$	$I4_1/amd$	Ga_2Hf	3.971		24.32	[37]
TiAl	*P*4/*mmm*	AuCu	3.976		4.049	[38]
Ti_3Al	$P6_3/mmc$	Ni_3Sn	5.77		4.62	[39]
$TiZn_{16}$	*Cmcm*	$TiZn_{16}$	7.72	11.44	11.75	[40]
$TiZn_8$						[31]
Ti_3Zn_{22}	$P4_2/mbc$	Ti_3Zn_{22}	11.523		11.456	[33]
$TiZn_7$						[30–32]
$TiZn_3$	*Pm*3*m*	$AuCu_3$	3.932			[41]
$TiZn_2$	$P6_3/mmc$	$MgZn_2$ (Laves phase)	5.064		8.210	[42]
Ti_2Zn_3						[31]
TiZn	*Pm*3*m*	CsCl	3.147			[43]
Ti_2Zn,	I4/*mmm*	$MoSi_2$	2.995		10.895	[44,45]

Table 2
Alloy and phase compositions (at.%).

No.	Nominal composition	Phase	Zn	Al	Ti
1	80Zn–12.5Al–7.5Ti	T	39.0	35.7	25.3
		Liq.Zn	97.6	2.4	N.D.[a]
2	90Zn–5Al–5Ti	$TiZn_{16}$	93.3	0.4	6.3
		T	49.1	25.5	25.4
		Liq.Zn	99.9	N.D.[a]	0.1
3	10Zn–70Al–20Ti	$TiAl_3$	3.6	72.1	24.3
		T	18.1	58.4	23.5
		α-Al	13.6	86.4	0.0
4	10Zn–63Al–27Ti	$TiAl_2$	3.2	63.6	33.2
		T	11.6	59.8	28.6
		$TiAl_3$	4.4	70.6	25.0
5	83Zn–5Al–12Ti	T	50.8	23.3	25.9
		$TiZn_{16}$	93.6	0.2	6.2
		$TiZn_8$	87.9	0.2	11.9
6	78Zn–3Al–19Ti	T	58.4	14.8	26.8
		$TiZn_8$	88.2	0.1	11.7
		TiZn	48.8	2.5	48.7
7	75Zn–1.5Al–23.5Ti	$TiZn_3$	71.6	1.7	26.7
		TiZn	48.9	2.1	49.0
		$TiZn_8$	88.6	N.D.[a]	11.4
8	57Zn–35Al–8Ti	T	28.4	47.0	24.6
		α-Al	20.1	79.6	0.3
		Liq.Zn	83.9	15.8	0.3

[a] N.D.: not detectable.

ence on Titanium. Since then substantial advances have been made in terms of theoretical models, computer software and hardware, allowing the calculation of extremely complex materials to be possible. In 1987, Murray [18] performed an elaborate assessment of the system. Due to the absence of experimental data, the boundaries of some phase fields were hypothesized. Afterward, Okamoto updated the phase diagram regularly [19,20]. Contradictions exist mainly regarding the formation of TiAl at high temperature. Some of these differences may be attributed to experimental difficulties. Nassik et al. [21] and Meschel and Kleppa [22] measured the enthalpy of formation for TiAl, $TiAl_2$, $TiAl_3$ and Ti_3Al phases by direct reaction calorimetry at high temperatures. These values agree very well with the calculations based on the electronic density functional theory (DFT) [23]. Recently, Raghavan [24] and Schuster and Palm [25] reassessed the Ti–Al system again. The latter critically re-evaluates all available literature data. The result of this assessment is accepted in this work. There are four intermediate phases in the system at 723 K, namely, $TiAl_3$ (75.0% Al), $TiAl_2$ (66.6% Al), TiAl (50.5–57.3% Al), and Ti_3Al (20.0–35.8% Al) (all compositions in at.% except otherwise noted).

The intermetallics existing in the Zn–Ti system are still in dispute even though numerous researchers have studied the Zn–Ti system [26–28]. Seven compounds, $TiZn_{15}$, $TiZn_{10}$, $TiZn_5$, $TiZn_3$, $TiZn_2$, TiZn, and Ti_2Zn, were suggested in the Murray's assessment [29]. However, Vassilev et al. [30,31] reported five additional compounds: $TiZn_{16}$, $TiZn_8$, Ti_3Zn_{22}, $TiZn_7$ and Ti_2Zn_3 by investigating the Zn-rich region of the phase diagram using diffusion couples, differential scanning calorimetry and X-ray diffraction. However, the existence of $TiZn_5$ and $TiZn_{10}$ could not be confirmed in these studies [30,31]. The researchers believe that the intermediate phases in the system are not necessarily all stoichiometry compounds and could exist in the vicinity of their respective stoichiometry, probably in metastable states [30]. Gloriant et al. [32] have found that the compound $TiZn_7$ was the only phase between $TiZn_{15}$ and $TiZn_3$. Chen et al. [33] performed rigorous structural analyses of $TiZn_{16}$ and Ti_3Zn_{22} using single crystal specimens and X-ray diffraction technique. They reported that no indications for an additional phase between $TiZn_3$ and Zn, other than Ti_3Zn_{22}

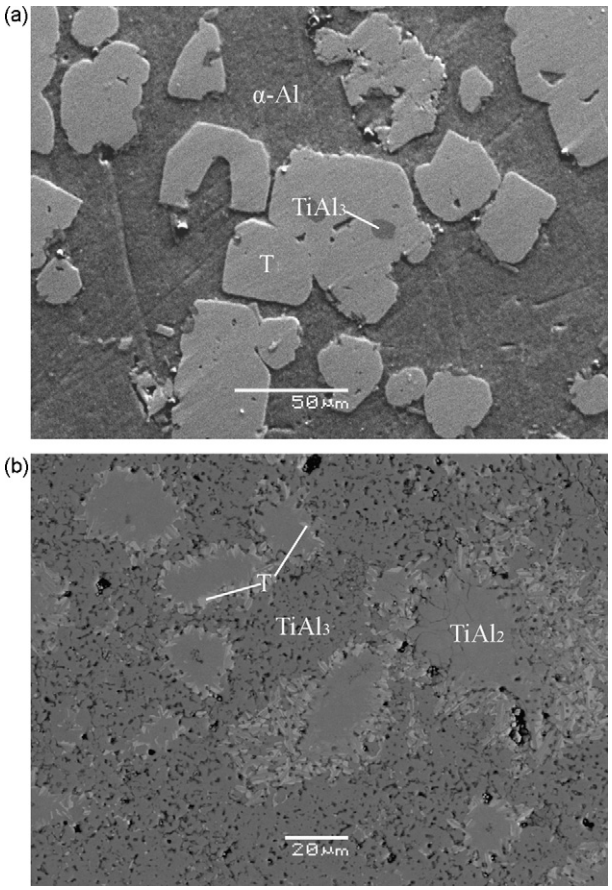

Fig. 2. (a) The microstructure of Alloy 3 consists of three phases: T + α-Al + $TiAl_3$. (b) Three phases, T, $TiAl_3$ and $TiAl_2$, showed on a backscattered electron (BSE) micrograph of Alloy 4.

Table 3
The tie-line data from diffusion couple (in at.%).

Diffusion couple	Phase	Zn	Al	Ti
$Ti_{25}Al_{75}$/Zn	$TiAl_3$	0.0	72.7	27.3
Tie-line 1	$TiAl_3$	0.7	72.9	26.4
	T	16.9	57.9	25.2
Tie-line 2	T	31.3	44.7	24.0
	Liq.Zn	99.3	0.7	N.D.[a]

[a] N.D.: not detectable.

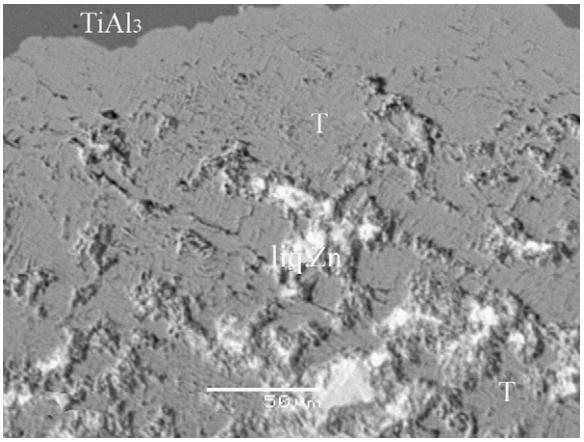

Fig. 3. Backscattered electron image (BSE) of diffusion couple $Ti_{25}Al_{75}$/Zn.

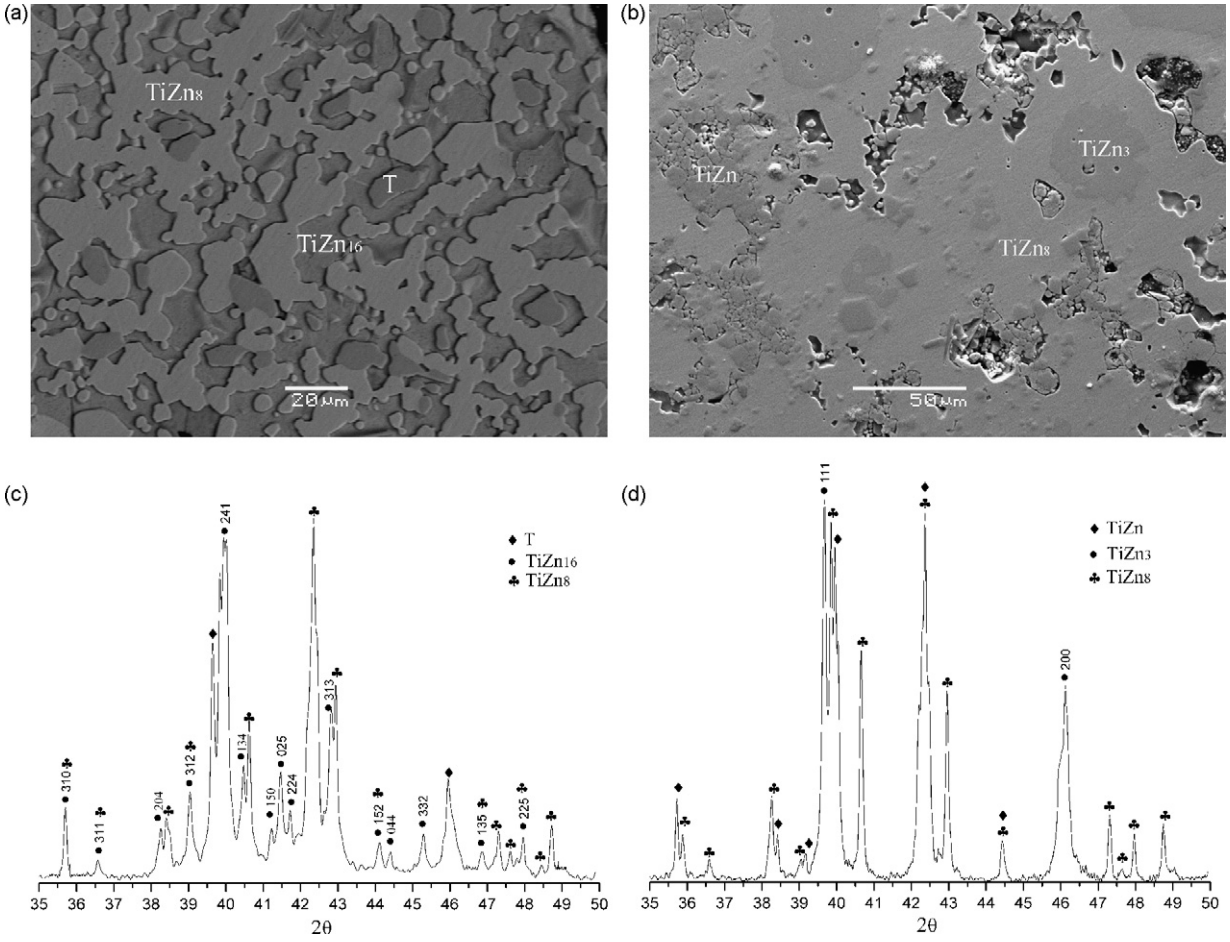

Fig. 4. SEM images and XRD patterns of the Alloys 5 and 7 annealed at 723 K for 30 days. (a) The microstructure of Alloy 5 corresponds to the three-phase equilibrium state: the T + $TiZn_{16}$ + $TiZn_8$. (b) SEM image of Alloy 7 corresponds to the three-phase equilibrium state of $TiZn_8$ + $TiZn_3$ + TiZn. (c) XRD pattern of Alloy 5. (d) XRD pattern of Alloy 7.

and $TiZn_{16}$ have been observed. The intermediate phase of Ti_3Zn_{22} is not necessarily believed to be stoichiometry compound and might be identical with $TiZn_7$ or with $TiZn_8$ considering the homogeneity range of the phase [33]. To further investigate the phase stability of binary Zn–Ti intermetallics, a recent research has been performed on both experimental colorimetric measurements and calculated heat of formation using electronic density functional theory (DFT) [34]. The results show that the calorimetric investigations agreed well with the corresponding ab initio values. Among the 48 intermetallics considered, $L1_2$-Ti_3Zn, $C11_b$-Ti_2Zn, B19-TiZn (CuTe-type), $L1_2$-$TiZn_3$, Ti_3Zn_{22}, and $TiZn_{16}$ are predicted to be stable at zero temperature [34]. The $L1_2$-Ti_3Zn has not been experimentally observed. However, the $C11_b$-Ti_2Zn, B19-TiZn, $L1_2$-$TiZn_3$, Ti_3Zn_{22}, and $TiZn_{16}$ phases are known to be stable to low temperatures.

Despite no study of the ternary system Zn–Al–Ti is reported, a recent work on the direct reaction calorimetry of several alloys along the $TiZn_3$–$TiAl_3$ section is performed [35]. X-ray diffraction and electron probe microanalysis suggested that $TiAl_3$ and $TiZn_3$ do not form a continuous solid solution as a two-phase mixture is observed in alloys near the TiAl edge [35].

Crystallographic data [33,36–45] of all binary compounds that form in the binary systems are shown in Table 1.

2. Experimental procedures

The Zn–Al–Ti isothermal section at 723 K was determined using equilibrated alloys with the aid of diffusion couple technique. For equilibrated alloys, a total of eight alloys were prepared using Zn block, Al wire and Ti powder. Fine Ti powder instead of Ti blocks was used to facilitate the diffusion reaction between Ti and Zn–Al alloy because the melting point of Ti is much higher than those of Al and Zn. The design compositions of the alloys are listed in the second column of Table 2. The purity of the metallic materials was all 99.99%. Samples were prepared by carefully weighing the Zn, Al and Ti, 3 g in total for each sample. All masses were weighed to an accuracy of 0.0001 g. Because of the high reactivity of Ti and Al, the Ti and Al were found to react with the quartz capsule at high temperature due to the extremely negative standard Gibbs energies of formation of the oxides [46,47]. As a result, the mixtures had to be contained in corundum crucibles which were then sealed in evacuated quartz capsules. Each alloy mixture was heated to above its estimated liquidus temperature and kept at this temperature for 16 h, followed by quenching in water using a bottom-quenching technique [48] to minimize Zn loss and to reduce sample porosity. The quenched samples together with their corundum crucibles were then sealed again and annealed at 723 K for 30 days to ensure the establishment of an equilibrium state. The treatment was completed with rapid water quenching to preserve the equilibrium state at 723 K.

In order to prepare the TiAl alloy/Zn diffusion couple, a Ti–Al binary alloy, viz. $Ti_{25}Al_{75}$ was prepared by melting pure elements in an arc furnace under high purity argon atmosphere using a non-consumable tungsten electrode. All metals had a purity of 99.99%. The ingot was remelted 5 times and kept at 1073 K for ten days to improve the homogeneity. Slices of 5 mm × 5 mm × 3 mm were cut from the button. Each slice was ground, polished and cleaned and then sealed together with appropriate amount of Zn. The sample was annealed at 723 K for 70 h, and then quenched in water.

The specimens were prepared in the conventional way for microstructure examination. A nital solution was used to reveal the microstructures of the samples. The conventional optical microscope was used for the examination of all the specimens. A JSM-6360LV scanning electron microscopy (SEM) equipped with an OXFORD INCA 500 wave dispersive X-ray spectroscope (WDS) was used to study the morphology and chemical composition of various phases in the samples. The phase makeup of the alloys was further confirmed by analyzing X-ray diffraction patterns generated by a Bruker D8 advanced X-ray diffractometer, operating at 50 kV and 100 mA with Cu Kα radiation.

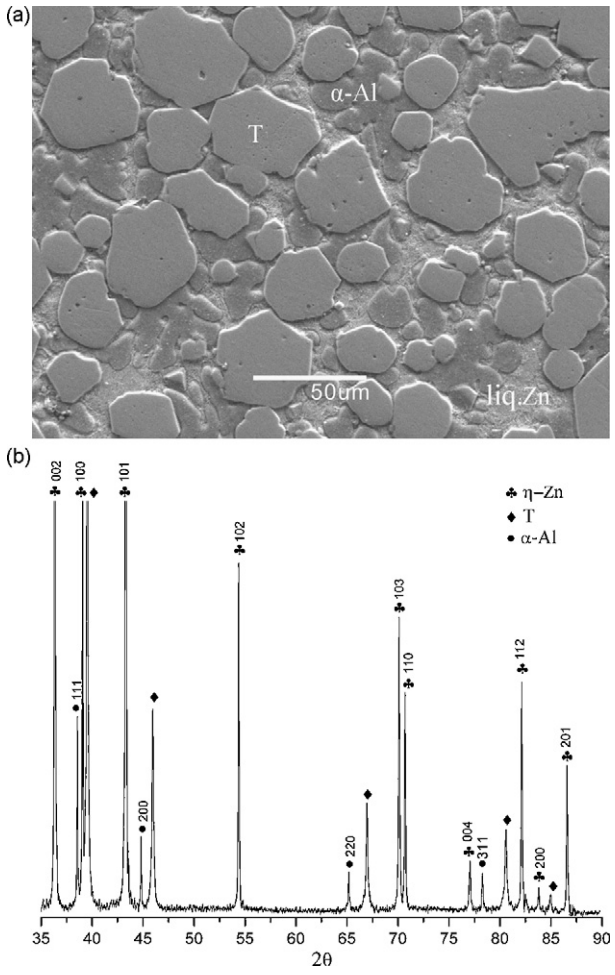

Fig. 5. The microstructure and XRD patterns generated from Alloys 8 confirm the T phase, α-Al phase and liq.Zn phase co-exist.

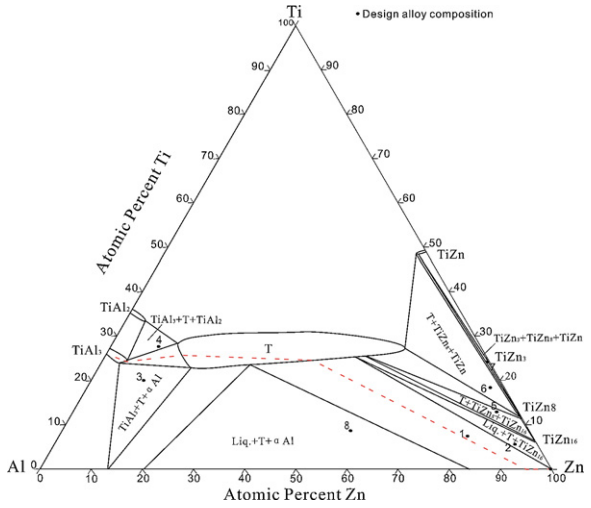

Fig. 6. The Zn-rich corner of the 723 K isothermal section of the Zn–Al–Ti phase diagram.

3. Results and discussion

Phases in alloys can be easily differentiated based on the relief, color and chemical composition. In most cases, the results obtained by SEM–WDS analysis alone are sufficient for phase identification. However, the true identities of the phases were all confirmed by analyzing the relevant X-ray diffraction patterns.

All phases found in the alloys are listed in Table 2 (column 3) together with the chemical compositions (columns 4–6) determined by the SEM–WDS technique. The compositions reported are the averages over at least five measurements. A new intermediate phase T which exists in a separate composition range was identified in these samples. The typical microstructure of the equilibrated alloys is presented in Fig. 1.

As can be seen in Fig. 1a, the microstructure of Alloy 1 consists of two phases, the T phase and liq.Zn phase. The gray matrix is marked as "liq.Zn" in Fig. 1a because it was in the liquid state at 723 K. The dark blocks belong to the ternary T phase. Ti was practically not detected in the liq.Zn phase. Alloy 2 consists of three phases: T, $TiZn_{16}$ and liq.Zn, as shown in Fig. 1b. T shows the most dark color among the three phases. WDS analyses revealed that the T phase contains 49.1% Zn, 25.5% Al and 25.4% Ti. The $TiZn_{16}$ phase and the T phase disperse in the matrix of the liq.Zn phase. The designation of $TiZn_{16}$ is based on the X-ray diffraction pattern analysis of the compound. The existence of $TiZn_{16}$ is first reported by Heine who published the X-ray diffraction pattern of this compound [43]. This compound has been included in the Zn–Ti phase diagram [31] proposed by Vassilev. The presence of this phase at 723 K substantiates the early finding that the peritectic temperature of its formation is 733 K [49,50], higher than the 718 K indicated by Massalski [46]. WDS analyses indicate that the solubility of Ti in the liq.Zn phase is 0.1% and that of Al in the $TiZn_{16}$ phase is 0.4%.

To further confirm the existence of the T phase, the X-ray diffraction patterns generated from Alloys 1 and 2 are shown in Fig. 1c and d. The results indicate that the phases in these alloys are corresponding to those determined by the SEM–WDS technique. The characteristic peaks of the T phase can be seen clearly in Fig. 1c for T phase is the major phase in Alloy 1. The patterns suggest that the strongest peak of the T phase locates at $2\theta = 39.6^{\circ}$. It can be seen that the lattice of the η-Zn phase is not noticeably distorted in this case and the three peaks of this phase are located at their normal positions.

Alloys 3 and 4 were prepared based on the Al-rich side of the phase region. The microstructure of Alloy 3 is shown in Fig. 2a. It can be seen that the microstructure of this alloy consists of three phases: T + α-Al + $TiAl_3$. The dark gray matrix appertains to the Al-rich phase α-Al. The gray blocks represent the ternary phase T. The dark area in the center or in the margin of the T phase corresponds to $TiAl_3$. WDS analyses reveal that the T phase contains 18.1% Zn, 58.4% Al and 23.5% Ti. This composition is different from that of the $TiAl_3$ phase, which has 3.6% Zn, 72.1% Al and 24.3% Ti. A comparison between Fig. 1a and b and Fig. 2a and b shows that the color of the T phase becomes lighter with the increase of Al content. A backscattered electron (BSE) micrograph of Alloy 4 is shown in Fig. 2b. It can be seen very clearly that the microstructure of this alloy corresponds to the ($TiAl_3$ + T + $TiAl_2$) three-phase equilibrium state. The white crystals distributing around the gray area appertain to the ternary phase T. The gray areas belong to the $TiAl_2$ and the matrix phase with lots of pore is $TiAl_3$. The maximum solubility of Zn in $TiAl_3$ and $TiAl_2$ is about 4.4% and 3.2%, respectively. The data listed in Table 2 indicate that the T phase has a relatively wide composition range. It contains Zn from 11.6 to 58.4%, Al from 14.8 to 59.8% and Ti from 23.5 to 28.6%.

The microstructure of a $Ti_{25}Al_{75}$/Zn diffusion couple annealed at 723 K for 70 h shown in Fig. 3 confirms the existence of the T phase again. It was found that zinc was exhausted in the diffusion couple at the end of anneal treatment. The tie-line data obtained with WDS from the diffusion couple are listed in Table 3. It can be seen from Fig. 3, the sequence of the phases that formed in the diffusion couple $Ti_{25}Al_{75}$/Zn is ($TiAl_3$) → (T + liq.Zn).

As indicated earlier, the prevailing Zn–Ti phase diagram [28] includes $TiZn_{10}$ and $TiZn_5$ without $TiZn_8$. However, $TiZn_8$ was substantiated in the phase diagram presented by Vassilev [31]. Chen et al. [33] reported the existence of Ti_3Zn_{22} and determined the crystal structure in detail. The exact composition of this phase is $Ti_{2.841}Zn_{22.159}$, which corresponds to the $TiZn_8$ phase. In the present work, the results of Chen et al. are accepted. Combining with wave dispersive spectrometric analysis in Table 2 and X-ray diffraction pattern analysis, the existence of $TiZn_8$ has been confirmed in the present study in Alloys 5–7. As shown in Fig. 4a, the microstructure of Alloy 5 corresponds to the ($TiZn_{16}$ + $TiZn_8$ + T) three-phase equilibrium state. The T phase is darker than the $TiZn_8$ phase and it shows the most resistant to etching among the three phases. As a result, it is easy to distinguish the T phase from the $TiZn_8$ phase based on their color and compositions. SEM–WDS analyses indicate that the solubility of Al in $TiZn_{16}$ and $TiZn_8$ are all 0.2% respectively. Alloy 6 locates in the three-phase region of T + $TiZn_8$ + TiZn. The solubility of Al in $TiZn_8$ is 0.1%. The existence of this three-phase equilibrium state makes the equilibrium between the T phase and the $TiZn_3$ phase impossible. So the $TiZn_3$ phase should be in equilibrium with TiZn phase and $TiZn_8$ phase which has been proved by the microstructure of Alloy 7 as shown in Fig. 4b. To further confirm the existence of the $TiZn_8$ phase, X-ray diffraction patterns generated from Alloys 5 and 7, shown in Fig. 4c and d, were carefully studied. With the removal of all peaks contributed by the T phase and $TiZn_{16}$ in Fig. 4a, a set of consistent X-ray pattern of the $TiZn_8$ phase can be found in Fig. 4b.

The microstructure and X-ray diffraction pattern of Alloy 8 are shown in Fig. 5, in which, the T phase, Al-rich solid solution α-Al phase and liq.Zn phase co-exist. The relief and compositions of these phases are significantly different. SEM–WDS analyses indicate that the solubility of Ti in α-Al and liq.Zn was all 0.3% respectively.

Based on the experimental results obtained in this study and the information of relevant binary systems in the open literatures, the Zn-rich corner of the Zn–Al–Ti isothermal section at 723 K was constructed, as shown in Fig. 6. The schematic representation of diffusion path is also shown in Fig. 6. The Zn-rich corner of the Zn–Al–Ti ternary system at 723 K consists of seven ternary phase regions, i.e. T + $TiZn_{16}$ + liq.Zn, T + $TiZn_{16}$ + $TiZn_8$, T + $TiZn_8$ + TiZn, TiZn + $TiZn_3$ + $TiZn_8$, T + liq.Zn + α-Al, T + α-Al + $TiAl_3$, T + $TiAl_3$ + $TiAl_2$. It should be mentioned here that four Ti–Zn compounds, namely, $TiZn_{16}$, $TiZn_8$, $TiZn_3$ and TiZn were found in the present investigation. Other Ti–Zn compounds, such as $TiZn_5$, $TiZn_{10}$, $TiZn_2$ and Ti_2Zn_3, as shown in the prevailing Ti–Zn binary phase diagram proposed by Massalski [28], were not detected in the present study.

4. Conclusions

Based on SEM–WDS analyses and X-ray diffraction studies, the Zn–Al-rich corner of the Zn–Al–Ti ternary system at 723 K was determined in the present work. The main findings are listed below:

(1) The T phase found in the section is a true ternary phase. The T phase has a very large composition range of Zn from 11.6 to 58.4%, Al from 14.8 to 59.8% and Ti from 23.5 to 28.6%.
(2) The T phase is in equilibrium with liq.Zn, $TiZn_{16}$, $TiZn_8$, TiZn, α-Al, $TiAl_3$, $TiAl_2$ respectively.
(3) Four Ti–Zn compounds, $TiZn_{16}$, $TiZn_8$, $TiZn_3$, and TiZn were found in the present work.

Acknowledgements

This work was supported by the Hunan Provincial Natural Science Foundation of China (No. 07JJ3097) and National Nature Science Foundation (Nos. 50671088, 50771089 and 50971111).

References

[1] A.R. Marder, Prog. Mater. Sci. 45 (2000) 191.
[2] R. Fratesi, N. Ruffini, M. Malavolta, T. Bellezze, Surf. Coat. Technol. 157 (2002) 34.
[3] J. Foct, P. Perrot, G. Reumont, Scripta Metall. Mater. 28 (1993) 1195.
[4] N.-Y. Tang, J. Phase Equilib. Differ. 29 (2008) 337.
[5] K.-K. Wang, L. Chang, D. Gan, H.-P. Wang, Thin Solid Films 518 (2010) 1935.
[6] G. Reumont, T. Gloriant, P. Perrot, J. Mater. Sci. Lett. 14 (1995) 752.
[7] G. Reumont, T. Gloriant, P. Perrot, J. Mater. Sci. Lett. 15 (1996) 445.
[8] J.D. Culcasi, P.R. Seré, C.I. Elsner, Surf. Coat. Technol. 122 (1999) 21.
[9] N.-Y. Tang, J. Phase Equilib. Differ. 17 (5) (1996) 396.
[10] J. Nakano, D.V. Malakhov, S. Yamaguchi, G.R. Purdy, Calphad 31 (1) (2007) 125.
[11] X.H. Tang, F.C. Yin, X.M. Wang, J.H. Wang, X.P. Su, N.-Y. Tang, J. Phase Equilib. Differ. 28 (4) (2007) 355.
[12] S.-L. Chen, Y.A. Chang, Calphad 17 (2) (1993) 113.
[13] J.L. Murray, Bull. Alloy Phase Diagram 4 (1) (1983) 55.
[14] S.A. Mey, G. Effenberg, Z. Metallkd. 77 (7) (1986) 449.
[15] S. Wasiur-Rahman, M. Medraj, Calphad 33 (2009) 584.
[16] V. Erkelenz, E. Metall. Erz. 20 (1923) 206.
[17] L. Kaufman, N. Nesor, Calphad 2 (1978) 325.
[18] J.L. Murray, Metall. Mater. Trans. A 9 (1988) 243.
[19] H. Okamoto, J. Phase Equilib. Differ. 14 (1993) 120.
[20] H. Okamoto, J. Phase Equilib. Differ. 21 (2000) 311.
[21] M. Nassik, F.Z. Chrifi-Alaoui, K. Mahdouk, J.C. Gachon, J. Alloys Compd. 350 (2003) 151.
[22] S.V. Meschel, O.J. Kleppa, in: J.S. Faulkner, R.G. Jordan (Eds.), Metallic Alloys: Experimental and Theoretical Perspectives, Kluwer, Dordrecht, 1994, p. 103.
[23] G. Ghosh, M. Asta, Acta Mater. 53 (2005) 3225.
[24] V. Raghavan, J. Phase Equilib. Differ. 26 (2005) 171.
[25] J.C. Schuster, M. Palm, J. Phase Equilib. Differ. 27 (2006) 255.
[26] S. Goto, K. Esashi, S. Koda, S. Morozumi, J. Jpn. Inst. Met. 37 (1973) 466.
[27] M. Saillard, G. Develey, C. Becle, J.M. Moreau, D. Paccard, Acta Crystallogr. B 37 (1981) 224.
[28] T.B. Massalski, Binary Alloy Phase Diagrams 3 (1990) 3501.
[29] J.L. Murray, Bull. Alloy Phase Diagrams 5 (1984) 52.
[30] G.P. Vassilev, X.J. Liu, K. Ishida, J. Alloys Compd. 375 (2004) 162.
[31] G.P. Vassilev, Z. Metallkd. 95 (2004) 813.
[32] T. Gloriant, G. Reumont, P. Perrot, Z. Metallkd. 88 (1997) 539.
[33] X.A. Chen, W. Jeitschko, M.E. Danebrock, C.B.H. Evers, K. Wangner, J. Solid State Chem. 118 (1995) 219.
[34] G. Ghosh, S. Delsante, G. Borzone, M. Asta, R. Ferro, Acta Mater. 54 (2006) 4977.
[35] S. Delsante, G. Ghosh, G. Borzone, Calphad 33 (2009) 50.
[36] P. Norby, A.N. christensen, Acta Chem. Scand. A 40 (1986) 157.
[37] H. Mabuchi, T. Asai, Y. Nakayama, Sci. Metall. 23 (1989) 685.
[38] P. Duwez, J.L. Taylor, J. Met. 4 (1952) 70.
[39] B. Goldak, B. Parr, Trans. Am. Inst. Min. Eng. 221 (1961) 639.
[40] L. Calvert, Victoria, Australia, Private Communication, 1990.
[41] P. Pietrokowsky, Trans. Am. Inst. Min. Eng. 200 (1954) 219.
[42] P. Pietrokowsky, Trans. Am. Inst. Min. Eng. 6 (1954) 219.
[43] W. Heine, U. Zwicker, Z. Metallkd. 53 (1962) 380.
[44] K. Schubert, K. Frank, R. Gohle, A. Maldonado, H.G. Meissner, A. Raman, Natuwissenschaft 50 (1963) 41.
[45] W. Rossteutscher, K. Schubert, Z. Metallkd. 56 (1965) 730.
[46] T.B. Massalski, Binary Alloy Phase Diagrams 2 (1990) 1785.
[47] R. Swalin, Thermodynamics of Solids, Wiley, London, 1961, p. 138.
[48] X. Su, N.-Y. Tang, J.M. Toguri, Can. Metall. Q. 40 (2001) 377.
[49] E. Gebhardt, Z. Metallkd. 33 (1941) 355.
[50] E.A. Anderson, E.J. Boyle, P.W. Ramsey, Trans. Am. Inst. Min. Eng. 156 (1944) 278.